# Hot deformation in nanocrystalline Nd–Fe–B backward extruded rings*

Li An-Hua(李安华)†, Zhao Rui(赵 睿), Lai Bin(赖 彬),
Wang Hui-Jie(王会杰), Zhu Ming-Gang(朱明刚), and Li Wei(李 卫)

*Division of Functional Materials, Central Iron & Steel Research Institute, Beijing* 100081, *China*

(Received 21 April 2011; revised manuscript received 13 June 2011)

Radially oriented Nd–Fe–B rings are prepared by backward extrusion of fine grained melt-spun powder. Melt-spun powder with the nominal composition of $Nd_{30.5}Fe_{bal.}Co_{6.0}Ga_{0.6}Al_{0.2}B_{0.9}$ (wt%) is used as starting material. The effects of process variables, such as deformation temperature ($T_d$), strain rate ($\dot{\varepsilon}$) and height reduction ($\Delta h\%$), on the magnetic properties of the rings are investigated. A scanning electron microscope (SEM) equipped with an energy spectrum device is used to study the metallograph and microfracture of the extruded rings. The $B_r$ and $(BH)_{max}$ reach the optimum values at $T_d = 800$ °C, $\dot{\varepsilon} = 0.01$ mm/s, and $\Delta h\% = 70\%$. It is found by SEM observations that the particle boundaries, which seemingly correspond to the interfaces of the starting melt-spun powders, emerge after the corrosion of metallography specimens. This is helpful for studying the effects of powder–powder interface on the local deformation and deformation homogeneity in the rings. For different spatial positions of the extruded rings, there are characteristic metallographies and microfractures. The upper end of the rings has the least deformation and worst texture, and therefore the worst magnetic properties. The magnetic properties in the radial direction increase slightly along the axis from the bottom to the middle, then steeply decrease at the upper end of the ring. The deformation and the formation-of-texturing processes are discussed. The deformation and the texturing formation of melt-spun Nd–Fe–B alloys probably involve grain boundary sliding and grain rotation, the solution-precipitation process and preferential growth of $Nd_2Fe_{14}B$ nanograins along the easy growth $a$-axis.

**Keywords:** radially oriented Nd–Fe–B rings, backward extrusion, microstructure, texture

**PACS:** 75.50.Ww, 62.20.F–, 62.25.–g **DOI:** 10.1088/1674-1056/20/10/107503

## 1. Introduction

Radially oriented Nd–Fe–B ring magnets are often applied to electric motors where high flux densities are required. Their major benefits include simpler construction, shorter response time and higher performance in a smaller package size.[1–4] Radially oriented Nd–Fe–B rings can be produced successfully by sintering. The crystal alignment is performed by an applied radially magnetic field. The radially oriented rings are also made of fine grained melt-spun powder by backward extrusion and the crystal alignment is performed by hot deformation. The hot extrusion method is especially advantageous in the case of the ring magnets with a small wall-thickness, small diameter and a high length-to-diameter ratio because the magnetic properties of these extruded magnets surpass those of sintered ones.[5]

Strip regions with coarse grains were found in the extruded rings, which were thought to start from melt-spun flake boundaries.[6] The melt-spun flake boundaries have an important influence on the deformation homogeneity, and therefore also on the texture and magnetic properties of the extruded rings. It is interesting to investigate the deformation and the microstructure of R–Fe–B backward extruded rings, which will help deepen the scientific knowledge and provide the basis of producing extruded rings with optimal texture and high magnetic properties.

## 2. Experiment

Melt-spun powder with the nominal composition of $Nd_{30.5}Fe_{bal.}Co_{6.0}Ga_{0.6}Al_{0.2}B_{0.9}$ (wt%) was used as the starting material. The powder was hot pressed into a fully dense precursor at 600 °–750 °C in vacuum. Radially oriented ring magnets with an outer diameter of 24.5 mm and an inner diameter of 18 mm were prepared by backward extruding the pressed precursor at 750 °C–900 °C under an argon atmosphere. The sketch maps of the fabrication processes of a backward

*Project supported by the National Natural Science Foundation of China (Grant Nos. 50804011 and 50931001).
†Corresponding author. E-mail: li_ah@sina.com
© 2011 Chinese Physical Society and IOP Publishing Ltd

extruded Nd–Fe–B ring are shown in Fig. 1. Scanning electronic microscope (SEM) equipped with an energy-dispersive X-ray spectroscopy (EDS) was used to investigate the metallography and the microfracture of the ring magnets. The phase composition analyses were performed by means of an energy spectrum system. The magnetic properties of the cut samples (1 mm×1 mm×2 mm) were measured with a vibrating sample magnetometer (VSM) in applied fields up to 30 kOe (1 Oe=79.5775 A/m) at room temperature. The crystal alignment was studied by means of X-ray diffraction with Cu $K\alpha$ radiation. The position dependences of the metallograph, the microfracture and the magnetic properties of the extruded Nd–Fe–Co–Ga–B rings were investigated. The deformation and the texture formation processes were discussed.

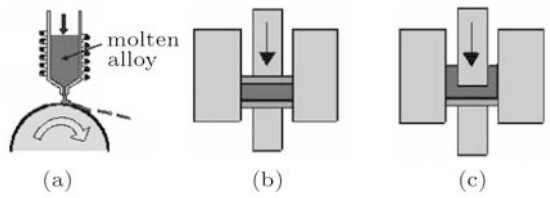



**Fig. 1.** Sketch maps of the fabrication processes of a backward extruded Nd–Fe–B ring: (a) melt spinning, (b) hot pressing in vacuum, and (c) hot deforming under $Ar_2$ atmosphere.

# 3. Results and discussion

## 3.1. Magnetic properties

The effects of process parameters on the magnetic properties of the hot deformed magnets were investigated. The magnetic properties of the magnets as functions of deformation temperature ($T_d$), strain rate ($\dot{\varepsilon}$) and height reduction (deformation ratio $\Delta h\%$), are shown in Figs. 2(a), 2(b) and 2(c), respectively. It is found that the remanence $B_r$ and the energy product $(BH)_{max}$ keep increasing up to $T_d$ = 800 °C, then slightly decrease with $T_d$ increasing; the coercivity ${}_iH_c$ reaches its maximum value at $T_d$ = 660 °C (see Fig. 2(a)). The $B_r$ and the $(BH)_{max}$ fast reach their maxima at the strain rate $\dot{\varepsilon}$ of 0.01 mm/s, while the ${}_iH_c$ obtains the maximum at $\dot{\varepsilon}$ = 0.03 mm/s (see Fig. 2(b)). It seems that the ${}_iH_c$ has different change tendencies from the $B_r$ and $(BH)_{max}$, varying with process parameter. The $B_r$ and the $(BH)_{max}$ increase with $\Delta h\%$ increasing, reach their maxima at $\Delta h\%$ = 70%, then nearly keep invariable up to $\Delta h\%$=80%, followed by a decrease with the further increase of $\Delta h\%$ (see Fig. 2(c)).

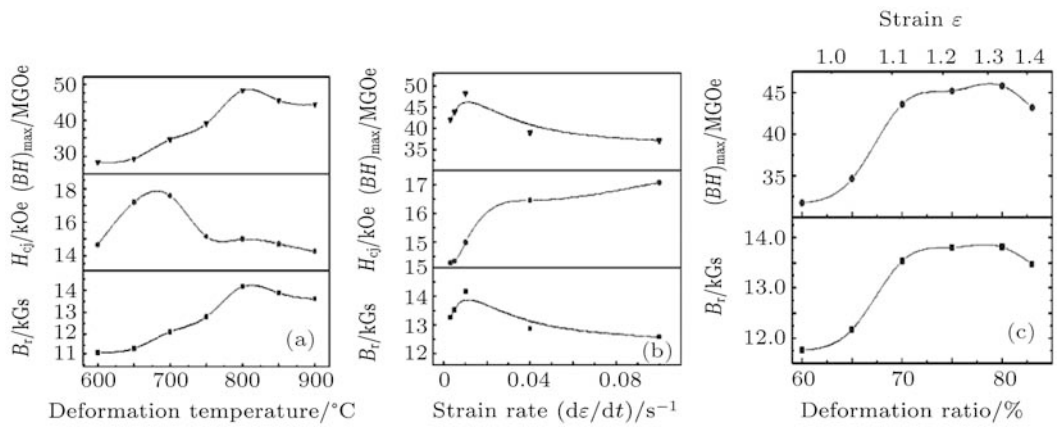



**Fig. 2.** Magnetic properties of the ring magnets and their variations with deformation temperature (a), strain rate (b), and deformation ratio (c), 1 Gs=$10^{-4}$ T, 1 Oe=79.5775 A/m, 1 MGOe=7.95775 kJ/m$^3$.

The magnetic properties in the radial direction of cubic samples cut from different axial positions of a backward-extruded ring were measured by a VSM. A $B_r$ of 13.0 kGs, ${}_iH_c$ of 6.26 kOe, and $(BH)_{max}$ of 34.40 MGOe have been obtained for the bottom sample. The magnetic properties increase slightly along the axis from the bottom to the middle. The magnetic properties of $B_r$ = 13.24 kGs, ${}_iH_c$ = 8.69 kOe, and $(BH)_{max}$ = 39.60 MGOe, have been achieved in the middle sample. The magnetic properties of the upper-end sample are $B_r$ = 9.15 kGs, ${}_iH_c$ = 15.90 kOe, and $(BH)_{max}$ = 17.59 MGOe. It can be seen that the $B_r$ and the $(BH)_{max}$ steeply decrease, while ${}_iH_c$ increases at the upper end of the ring. The magnetic properties of the upper end are very close to those of the isotropic pressed precursor. It suggests that the extruded ring approximately should retain the initial structure at its upper end, which is also confirmed by the XRD and SEM results.

### 3.2. SEM microstructure

SEM metallographs of the extruded ring are shown in Figs. 3(a) and (b). Here the particle boundaries seemingly start from the boundaries of the starting melt-spun flakes (namely the grain-coarsened strips shown in their microfractures, see Fig. 3). The particle size is on the order of 10 μm.

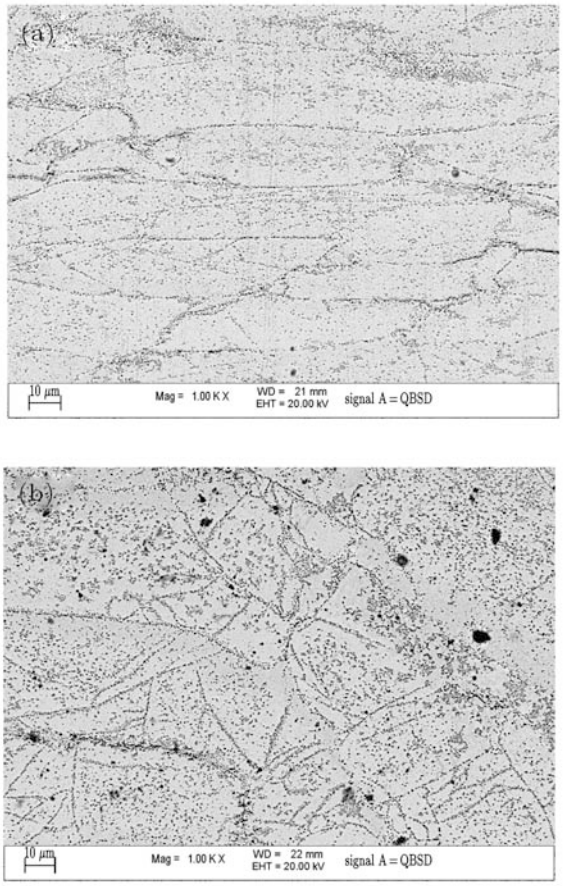



**Fig. 3.** Typical SEM metallographs in the middle (a) and the upper end (b) of an extruded Nd–Fe–B ring.

The particle boundaries are composed of many small holes resulting from the corrosion during specimen preparation. It is probable that because the melt-spun flake boundaries with disordered atom arrangement are in a high-energy status, they are corroded more easily than other parts. For different spatial positions, there are different characteristic morphologies in metallography. The elongated particles are found in the middle (see Fig. 3(a)) and the random particles in the upper end (see Fig. 3(b)) of the extruded Nd–Fe–B rings. Figure 4 shows an enlarged SEM metallograph of the local area in Fig. 3.

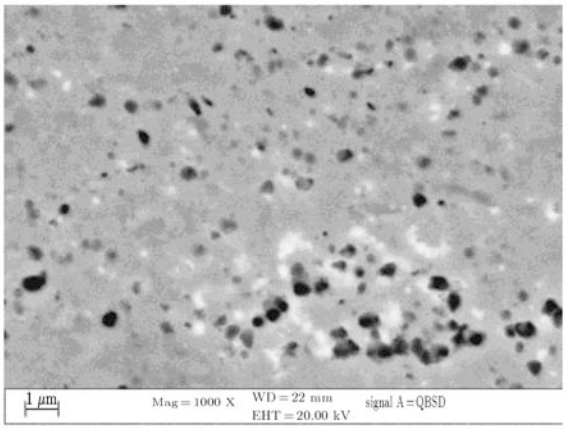



**Fig. 4.** SEM metallograph of the locally enlarged area in Fig. 3.

**Table 1.** EDAX results of phases in Fig. 4 (at%).

| Compositions | Fe | Co | Nd |
|---|---|---|---|
| Grey phase | 77.78 | 6.34 | 15.88 |
| White phase | 54.53 | 0.97 | 44.60 |
| Black spot | 78.45 | 7.18 | 14.37 |

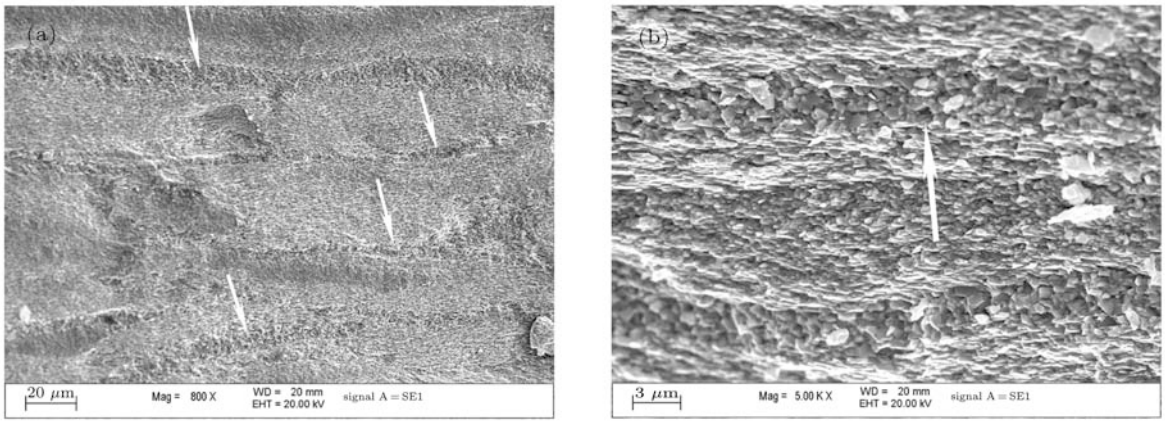



**Fig. 5.** SEM microfractographs in low magnification (a) and high magnification (b) of the cross section of the rings, the grain-coarsened strips were found as indicated by white arrows.

SEM microfractographs of the extruded ring in low and high magnifications are shown in Figs. 5(a) and 5(b), respectively. The grain size of an extruded ring is on the order of 100 nm. As indicated by white arrows, the typically periodic grain-coarsening regions were found, which were thought to start from melt-spun flake boundaries.[6] The different microfracture characteristics were found at different spatial positions: flake-shaped grains for the inner, elongated grains for the middle and particle-shaped grains for the outer region in the cross section. Only particle-shaped grains were observed at the upper end of the ring.[7] The upper end of the rings has the worst crystal alignment, so the worst magnetic properties.

### 3.3. Mechanisms of deformation and texture-forming

Regarding the deformation and the texture formation processes of melt-spun Nd–Fe–B alloys, all microstructural investigations confirm the absences of dislocations, sliding lines and twins.[8−10] In other words, the transgranular deformation models is not applicable to the melt-spun Nd–Fe–B alloys. Therefore, the intergranular deformation models are emphatically considered. Due to the presence of the grain-boundary phase with low melting point and also the high activation of grain-boundary atoms at high temperature, the grain boundary sliding and the grain rotation are conceivable under the compressive stress (see Fig. 6). The solution-precipitation process is used to explain the deformation of melt-spun Nd–Fe–B alloys.[6] In the geological literature the term "pressure solution" is used for a similar phenomenon (see Fig. 7).[11] The liquid phase speeds up the deformation process. The texture formation in Nd–Fe–B melt-spun alloys can originate from the anisotropies of the elastic properties and strain energy.[12] The grains with the $c$ axis parallel to the press direction have the lowest strain energy. The applied pressure causes only grains with the $c$ axis parallel to the press direction to be allowed to grow. The deformation and the texture formation of melt-spun Nd–Fe–B alloys probably involve grain boundary sliding grain rotation, solution precipitation and preferential growth of $Nd_2Fe_{14}B$ nanocrystalline grains along the easy growth $a$-axis.

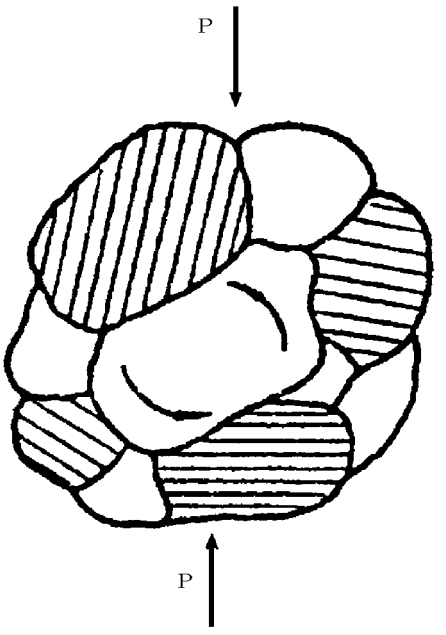



**Fig. 6.** Sketch maps of grain-boundary sliding and grain rotation activated at high temperature under the compressive stress.

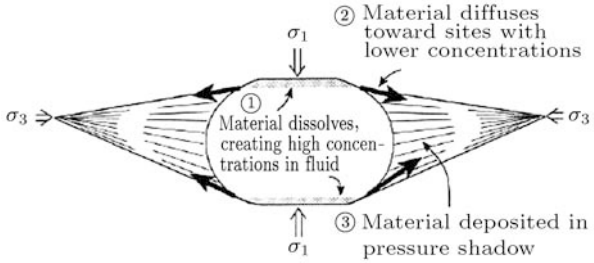



**Fig. 7.** Illustration of pressure solution with adding water (or liquid) to speed up the process.[8]

## 4. Conclusions

Radially oriented Nd–Fe–B ring magnets are prepared by the backward extrusion of melt-spun powder. The effects of deformation temperature, strain rate and height reduction on the magnetic properties of the deformed magnet are investigated. The position dependences of the microstructures and the magnetic properties of the extruded rings are discussed. The $B_r$ and the $(BH)_{max}$ reach their optimum values at $T_d = 800$ °C, $\dot{\varepsilon} = 0.01$ mm/s, and $\Delta h\% = 70\%$. It is found by SEM observations that the particle boundaries, which are seemingly correspond to the interfaces of the starting melt-spun powders, emerge after the corrosion of the metallography specimen. It is helpful for clarifying the effects of powder–powder interface on local deformation and deformation homogeneity in the rings. For different spatial positions of the extruded ring, there are the characteristic metallographies and microfractures. The upper end of the ring has the minimal deformation and worst texture, so the worst magnetic properties. The magnetic properties in the radial direction increase slightly along the axis from the bottom to the middle, then steeply decrease at the upper end of the ring. The deformation and the formation-of-texturing processes are discussed. The deformation

and the texturing formation of melt-spun Nd–Fe–B alloys probably involve the grain boundary sliding the grain rotation, the solution-precipitation process and the preferential growth of $Nd_2Fe_{14}B$ nanograins along the easy growth $a$-axis.

# References


[1] Hinz D, Kirchner A, Brown D N, Ma B M and Gutfleisch O 2003 *J. Mater. Process. Technol.* **135** 358

[2] Li X M, Fang Y K, Guo Z H, Liu T, Guo Y Q, Li W and Han B S 2008 *Chin. Phys.* B **17** 1674

[3] Huang W G, Zhang X Q, Li G K, Sun Y, Li Q A and Cheng Z H 2009 *Chin. Phys.* B **18** 5034

[4] Zhao J J, Xing R, Lu Y, Haosibayar Y, Zhao M, Jin X, Zheng L, Ning W, Sun Y and Cheng Z H 2008 *Chin. Phys.* B **17** 2717

[5] Yoshikawa N, Iriyama T, Yamada H, Kasai Y and Panchanathan V 1999 *IEEE Trans. Magn.* **35** 3268

[6] Grünberger W, Hinz D, Kirchner A, Müller K H and Schultz L 1997 *J. Alloys Compd.* **257** 293

[7] Li A H, Li W, Lai B, Wang H J, Zhu M G and Pan W 2010 *J. Appl. Phys.* **107** 09A725

[8] Lee R W, Brewer E G and Schaffel N A 1985 *IEEE Trans. Magn.* **21** 1958

[9] Mishra R K, Chu T Y and Rabenberg L K 1990 *J. Magn. Magn. Mater.* **84** 88

[10] Mishra R K, Panchanathan V and Croat J J 1993 *J. Appl. Phys.* **73** 6470

[11] Green H W 1984 *J. Geophys. Res.* **89** 4313

[12] Li L and Graham C D 1992 *IEEE Trans. Magn.* **28** 2130